Fatigue Crack Propagation in CA6NM/AWS410NIMO FCAW and GTAW Welded Joints

Anderson Geraldo Marenda Pukasiewicz, anderson @utfpr.edu.br
UTFPR universidade Tecnológica Federal do Paraná - Campus Ponta Grossa, Av. Monteiro Lobato s/n, km04, Ponta Grossa, Paraná, Brasil, CEP 84016-210
Sérgio Luiz Henke, henke@lactec.org.br
André Ricardo Capra, andre.capra@lactec.org.br
LACTEC, Instituto de Tecnologia para o Desenvolvimento, Curitiba, Paraná, Brasil,
Av. Lothário Meissner, nº01, Jardim Botânico, Curitiba, Paraná, Brasil, CEP 80210-170

Abstract*. CA6NM steel used in hydraulic turbines showed adequate resistance to cavitation erosion and good weldability, otherwise, presents restrictions in the welding zone and HAZ. The purpose of this work is to evaluate the fatigue crack propagation in FCAW and GTAW under distinct interpass temperature control in CA6NM welded joints and compare to BM (base metal). Additionally, the mechanisms of crack propagation were characterized. The welded joints were evaluated through da/dN-ΔK and by Paris law coefficients C and m. Welded joints were characterized using microhardness profile, metallography and scanning electron microscopy, SEM. The results indicated that fracture mechanisms were characterized by fatigue striations and dimpled fracture in FCAW, and fatigue striations in GTAW welded joints. The fracture mechanisms in the BM were intergranular, fatigue striations and dimpled fracture. The constants C and m were 1,22,10^{-8} and 2,63 for BM, 7.83,10^{-11} and 3,82 for FCAW-HAZ, 2.470,10^{-10} and 3,80 for FCAW-WM, respectively. For GTAW WM, with 150ºC of interpass temperature, the constants C and m were 4,96.10^{-9} and 2,87 and for HAZ were 3,553.10^{-9} and 2,87, and for GTAW, with 80ºC of interpass temperature, the constants C and m were 1,746.10^{-8} and 2,54 and for HAZ are 2,146.10^{-9} and 3, 04. Slag inclusions in the FCAW were responsible for differences in fatigue crack propagation behavior compared to GTAW process.*

Keywords: *fatigue crack propagation; martensitic stainless steel; welding.*

1. Introduction

Since the 1960', soft martensitic stainless steels have been used to manufacture hydraulic turbine. These steels contain 12 - 13% of chrome, 2 - 5% of nickel and less than 0,06% of carbon in their chemical compositions. It is reveal high yield strength, excellent toughness, high resistance to cavitation and good weldability. Martensitic steels with low carbon content, such as the CA6NM steel, are always used in quenched and tempered conditions (Bilmes, *et al.* 2000).

Excellent toughness of these steels is due to the formation of fine dispersion of austenite among the martensite laths, during tempering treatment in temperatures in the order of 600°C, Figure 1 (Folkhard, 1988). Although the good weldability and less demanding requirements with regard to pre-heating and interpass temperature control, the weld metal (WM) and the heat affected zone (HAZ) show lower impact energy and fracture toughness than CA6NM base material (BM). The decrease in impact energy and fracture toughness occurs due to the reduction in the austenite content, which promotes hard and brittle microstructure, and defects, such as porosity and inclusions slag (Akhtar and Brodie, 1979).

Turbine runners in hydraulic power plants experience a combination of low-cycle fatigue, from the operational start-stop and high-cycle fatigue, due to hydraulic fluctuation and vibration cycles, combined with high static loads. Cracks can initiate from service on manufacturing defects and can propagate when the vibration loading exceeds the fatigue crack threshold. Hydraulic turbine runners develop fatigue cracks in areas where stress concentration and material defects coincide, this is the case of welded areas in high-pressure Francis turbine runners (Huth, 2005).

With the objective to obtain the balance between performance, mechanical integrity and cost, the turbine designers have tools to reliable prediction of fatigue crack growth. The fatigue crack size and crack growth rate can be estimated by linear elastic fracture mechanics, which can provide the stress field and stress factor intensity calculation during the crack propagation (Huth, 2005).

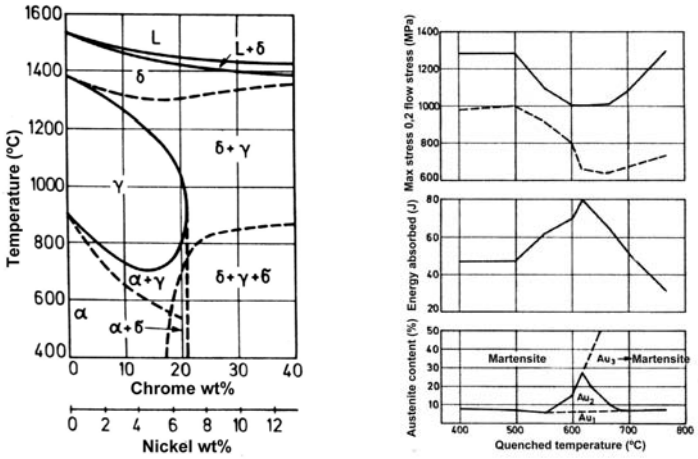

(a) (b)

Figure 1 Iron-Chrome-Nickel phase diagram for 3:1 Cr/Ni ratio (a), tempering temperature influence in austenite content and mechanical properties (b) (Folkhard, 1988).

At the moment, fatigue and fracture tests are undertaken in accordance with standards and codes developed by different institutions such as the American Society for Testing and Materials (ASTM) and the British Standards Institution (BSI). These tests were originally developed for use with homogeneous test samples and based on the concepts of *S-N*, *ε-N* and *da*/*dN*-Δ*K* for evaluation fatigue behavior. In order to carry out these tests in welded joints, various techniques and recommendations were suggested for preparing and evaluating the results, since it involves microstructure variations in small areas, and contain complex distributions of residual stress. A more detailed study of the fatigue behavior in welded joints is necessary to obtain the structure resistance (Moltubakk, 1999).

The purpose of this work is to evaluate the fatigue crack propagation in FCAW and GTAW with two different interpass temperatures in CA6NM welded joints. Additionally, the mechanisms of cracks propagation were characterized.

2. Experimental procedures

The material used was a soft martensitic stainless steel, CA6NM, 1050ºC air quenched and 580ºC tempered, supplied by Voith Siemens company. The chemical composition of the CA6NM steel, AWS E410NiMoT FCAW and ER410NiMo GTAW filler metals are presented in the Table 1. The FCAW and GTAW parameters are visualized in the Table 2. In GTAW, two interpass temperature were evaluated; 150ºC, close to the final martensite temperature transformation and 80ºC, under the final martensite temperature transformation.

Table 1. Chemical composition.

	ϕ (mm)	C (wt%)	Mn (wt%)	Cr (wt%)	Ni (wt%)	Mo (wt%)	P (wt%)	S (wt%)
CA6NM		0,02	0,64	12,4	3,7	0,42	0,008	0,0018
FCAW wire	1,6	0,026	0,33	10,5	3,6	0,45	0,019	0,0084
GTAW	2,5	0,017	0,42	12,1	4,35	0,49	0,023	0,001

Table 2. FCAW and GTAW parameters.

	Arc Tension (V)	Arc Current (A)	Welding Speed (cm/min)	Shielding gas	Shielding gas flow (l/min)	Interpasse temperature (ºC)
FCAW	25,6	320	29,5	Ar 8%CO_2	12	150
GTAW1	15,6	170	4,5	Ar	17	80
GTAW2	15,6	170	4,5	Ar	17	150

The dimensions of the welded pieces by FCAW were 200x70x20 mm, with a 40° chamfer and a K type joint. The GTAW uses a CA6NM piece machined to simulate a joint with 110x70x20mm, with a U type of joint. The welded joints and compact tension (CT) location are presented in Figure 2.

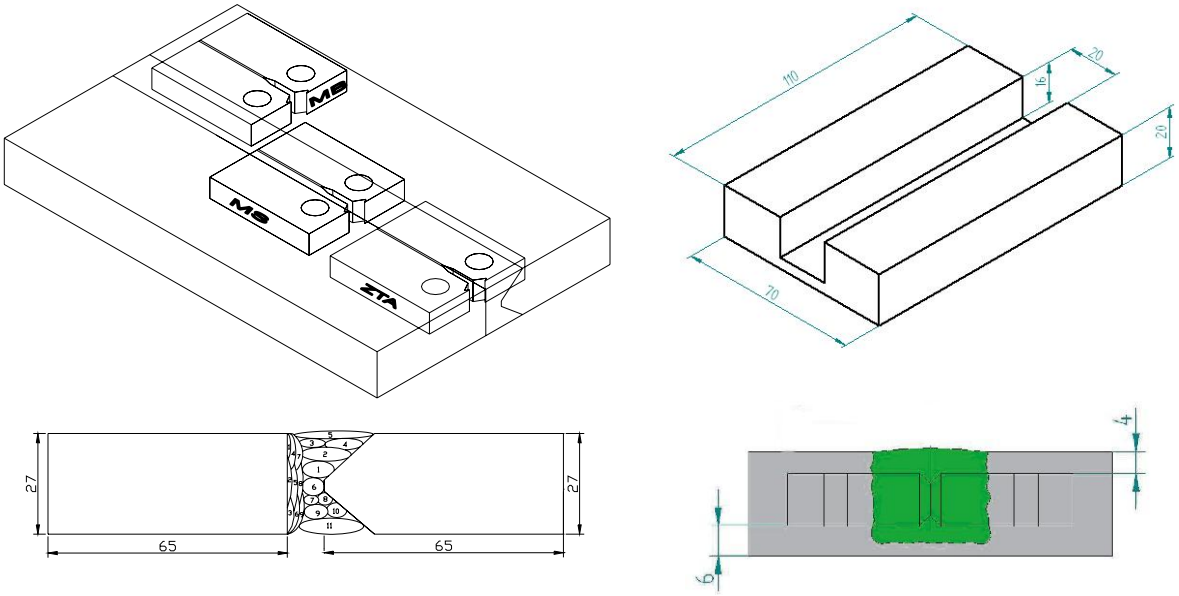

(a) (b)

Figure 2. Disposition of the test specimens in a FCAW (a) and GTAW (b) welded joint.

The fatigue crack growth tests were carried out in accordance with standard ASTM E647-95 using an Instron 8500 Plus dynamic test machine with servo-hydraulic action at room temperature. A frequency of 20 Hz with constant load amplitude and senoid curve was used, with a constant R stress ratio equal to 0,1 (ASTM E647–95a).

The fatigue crack propagation tests were carried out on CT type samples using side grooves to ensure crack propagation along a single plane. The crack growth is monitored by a compliance method using a clip-on crack opening displacement gauge. Compact tension samples, Figure 3, were aligned parallel to the welding direction. For evaluating the fatigue behavior of the HAZ, the pre-crack was put in a distance of approximately 1,0 mm of the fusion line. A substantial number of specimens were discarded since they had not met this requirement. After removing the samples, they were analyzed using Philips XL30 scanning electron microscope (SEM) to identify the fracture mechanisms involved.

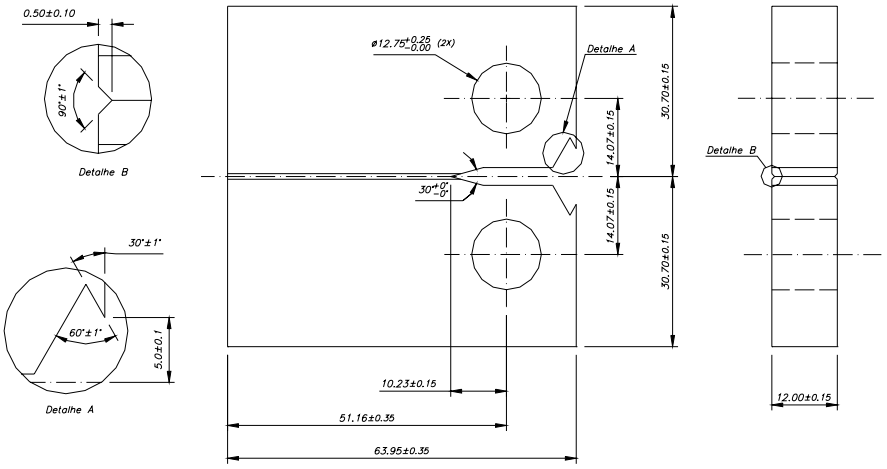

Figure 3. CT specimen dimensions.

3. Results and discussion

The microstructure of the FCAW and GTAW welded joint is seen in Figure 4. It can be seen that no grain growth occurred along the fusion line in the FCAW HAZ and GTAW HAZ, as shown in Figure 4, due to the low temperature Ac_4 ($\gamma \leftrightarrow \delta$), which promotes grain size refinement close to the fusion line (Folkhard, 1988, Pukasiewicz, 2002). The welded microstructures are visualized in Figure 4.

The microhardness profile in FCAW joint is seen in Figure 5(a), it can be visualized that hardness drops suddenly in the FCAW HAZ and do not present region with hardness higher than WM. The average hardness of the FCAW weld metal is 350 HV, and the base metal is 295HV. The hardness reduction in HAZ occurs because of the high input energy,

used in this welded joint, that reduce the cooling rate and promotes a tempering of the martensite with austenite precipitation, observed with polarized light, which increase the ductility and reduces the hardness. The high heat input in the FCAW was applied to reduce the quantity of slag inclusions, present in the weld zone, introduced by the flux inside the wire. Several samples were prepared and the reduction was more satisfactory with 320A of arc current.

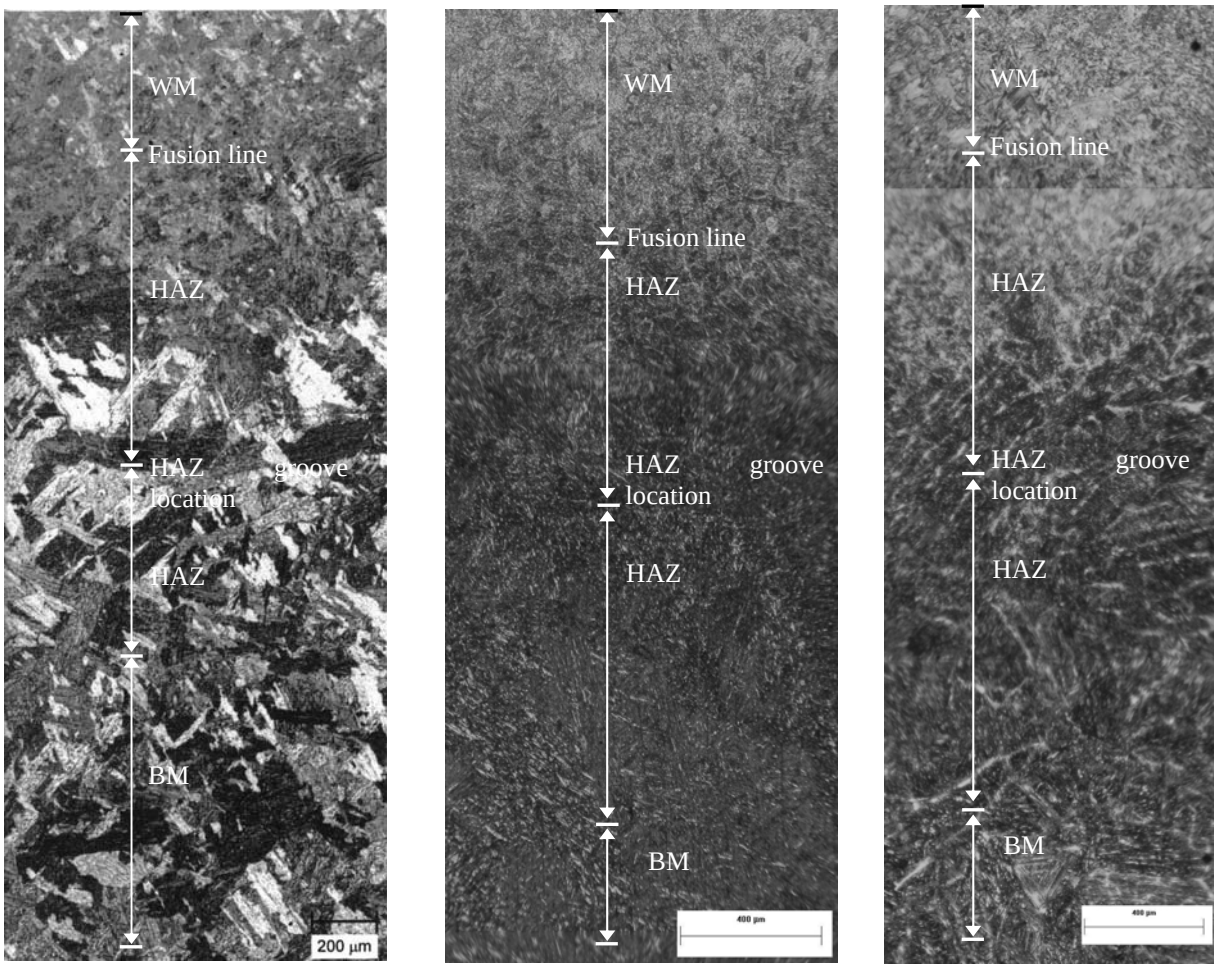

Figure 4. Weld micrographs, (a)FCAW, Villela, polarized light, (b) . 80ºC GTAW, (c) 150ºC GTAW.

The weld hardness profiles are illustrated in Figure 5, (a) for FCAW joint and (b) for GTAW joints.

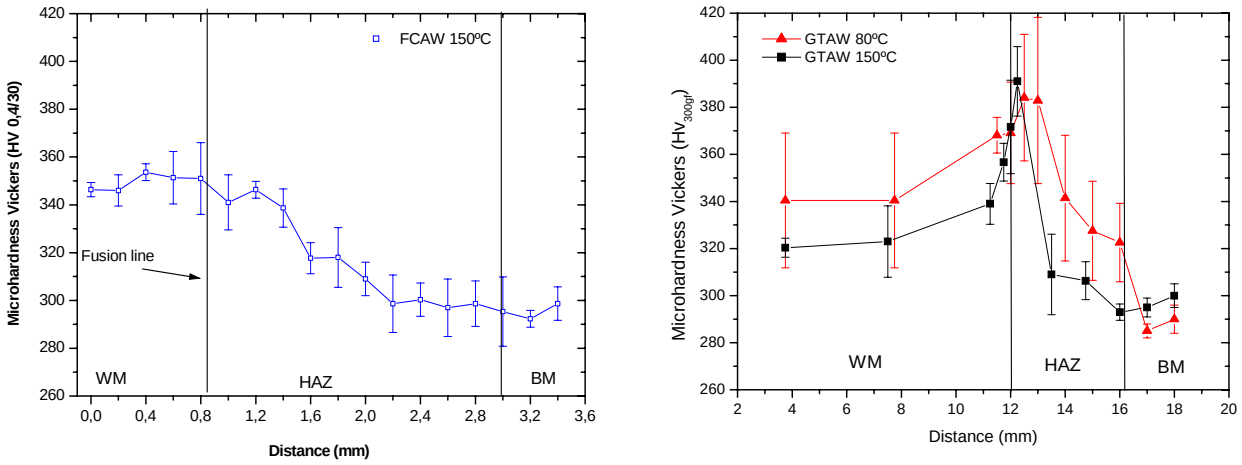

(a) (b)

Figure 5. Hardness profile in the FCAW weld, (a), and GTAW (b).

The microhardness profile in GTAW welded joints indicated that the sample with 80 ºC interpass temperature is harder than the sample welded with 150 ºC of interpass temperature, same behavior was observed in GTAW HAZ. This behavior occurred by the higher cooling rate occurred in the sample with lower interpass temperature control.

The fatigue crack propagation, da/dN x ΔK, behavior for WM, compared with BM, can be seen in Figure 6, whereas in Figure 7, the HAZ fatigue crack propagation, da/dN x ΔK, compared with CA6NM base metal can be observed. The results for the constants C and m of the Paris law, Equation (1), are visualized in Table 3.

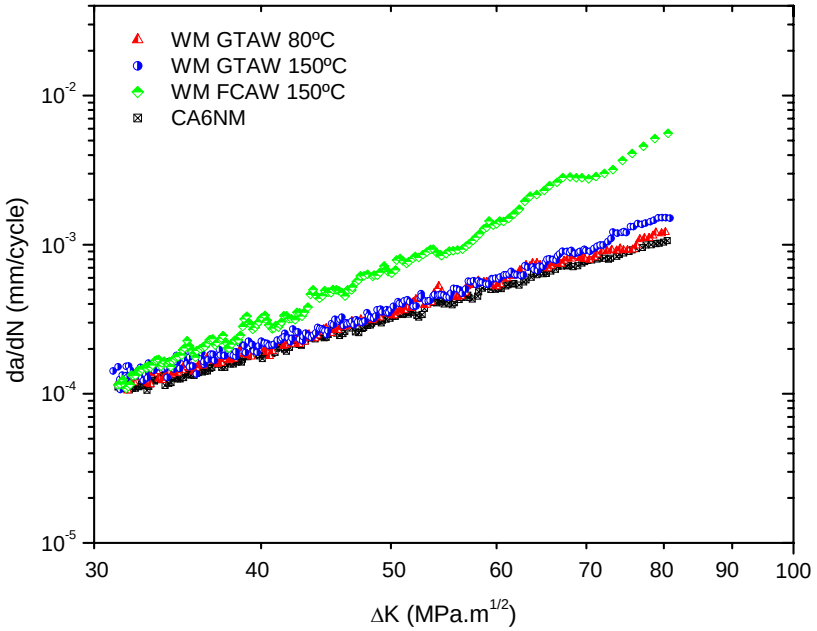

Figure 6. Fatigue crack growth of the CA6NM steel welded joint.

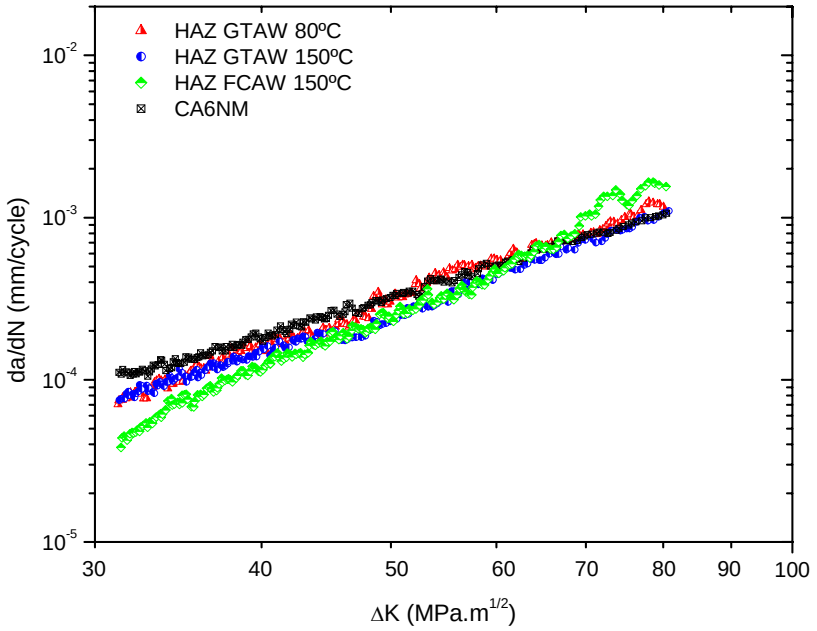

Figure 7. Fatigue crack growth of the CA6NM steel HAZ.

$$da/dN = C\Delta K^{m} \quad (1)$$

Table 3. Results of *C* and *m* materials constants of the Paris Law.

Samples	*C(mm/cycle)*	*m*
FCAW WM	$2{,}470x10^{-10}$	3,80
GTAW WM 80ºC	$1{,}746x10^{-08}$	2,54
GTAW WM 150ºC	$4{,}956x10^{-09}$	2,87
FCAW HAZ	$7{,}837x10^{-11}$	3,82
GTAW HAZ 80ºC	$2{,}146x10^{-9}$	3,04
GTAW HAZ 150ºC	$3{,}553x10^{-9}$	2,87
CA6NM	$1{,}224x10^{-8}$	2,63

Welding residual stress superimposed on the applied stress promotes crack-tip stress intensity factor different from that imposed by the servo-hydraulic machine, therefore the real stress intensity factor in the crack-tip is difficult to be analyzed (ASTM E647–95a). During samples preparation and pre-cracking growing stage, the welding residual stress are changed, resulting in more difficulty to analyze its influence on fatigue crack growth rates, so the welding residual stress can not be superimposed to applied ΔK. Samples preparation can relieve tensile residual stress and promote compressive residual stress on the specimen during milling and grinding operation (Shi, *et al.* 1990, Kang, *et al.* 1990, Shanmugam, *et al.* 2009).

The most important parameter in fatigue crack growing tests is the Paris-Erdogan exponent, *m*, which indicates how fast the fatigue crack growth is in tested material. Crack growth exponent '*m*', from de Equation (1) was obtained from the slope of the da/dN x ΔK range between 35 and 70 MPa$\sqrt{m}$ for all samples. If this exponent is lower, the resistance offered by the material to the fatigue crack growth will be higher and the fatigue life will bee longer also. Whether the exponent '*m*' is higher, the resistance offered by the material to the fatigue crack growth will be lower.

For intermediate values of ΔK larger straight-line inclinations, in the samples located in the FCAW HAZ and WM, in comparison to CA6NM BM and GTAW welded joints was observed. Fatigue crack growth rate in GTAW WM shows similar behavior to CA6NM base metal, Figure 7 and Table 3. The fatigue crack growth exponent '*m*' in FCAW HAZ is larger than CA6NM, with crack growth rate lower until approximately 62 MPa$\sqrt{m}$. Same behavior is observed in GTAW HAZ with 80ºCof interpass temperature control, similar results are described in the literature (Lee, *et al.* 2000, Tsay, *et al.* 2001). Greater *m* exponent was obtained in FCAW, HAZ and WM regions, in relation to GTAW, which represents lower fatigue crack growth resistance in FCAW welded joint.

The interpass temperature influence on GTAW welded joint can be observed differently in WM and HAZ fatigue crack growing resistance. Lower interpass temperature, 80ºC, promotes an increase in fatigue resistance to WM. Similar results are observed in T410S joints GMAW welded with AWS309L filler metal (Sánchez-Cabrera, *et al.* 2007). However, lower interpass temperature promotes a higher cooling rate in HAZ, promoting an increase in fatigue crack growth rate in GTAW HAZ welded with 80ºC of interpass temperature if compared with GTAW 150ºC welded joint.

With the intention to verify the fracture mechanisms which occurred during fatigue crack propagation in welded joints, SEM observation was carried out on the surface fracture. In Figure 8 fracture surface morphology of tested samples in low ΔK is observed. These fracture surfaces correspond to 2,0mm from pre-crack fatigue tip, between 18 and 30 MPa$\sqrt{m}$ the beginning of the fatigue crack growing curve. In beginning of the fatigue tests, the predominant fracture mechanism is highly facetted fracture planes, with small quantity of the intergranular fracture type in BM, while for FCAW and GTAW HAZ and WM is verified only facetted fracture planes. Fatigue striations or quasi-cleavage were not clearly visible in these fracture planes. It can be observed that in GTAW 80ºC HAZ and WM the fracture surface is more refined, which can be a higher cooling rate consequence occurred in this welded joint.

In Figure 9 changes can be visualized in fracture mechanisms, promoted by the increasement in crack-tip ΔK during crack growth. This corresponds to a fatigue crack length from 2,0mm to 23,0mm of tested samples. For CA6NM steel a 30 MPa$\sqrt{m}$ transition is observed with an absence of intergranular fracture, which is only observed fatigue patches separated by steps, Figure 9(a), containing fatigue striations, Figure 9(b).

Fracture mechanisms variations were observed in FCAW WM sample with 30 MPa$\sqrt{m}$, Figure 9(c) and (d), where equiaxed dimples were identified in some areas. These dimples were not common in ductile materials in low ΔK regime. These dimples are formed in consequence to the high concentration of slag inclusions. The samples located in the FCAW HAZ, GTAW WM and HAZ did not show any alteration in the fracture mechanism.

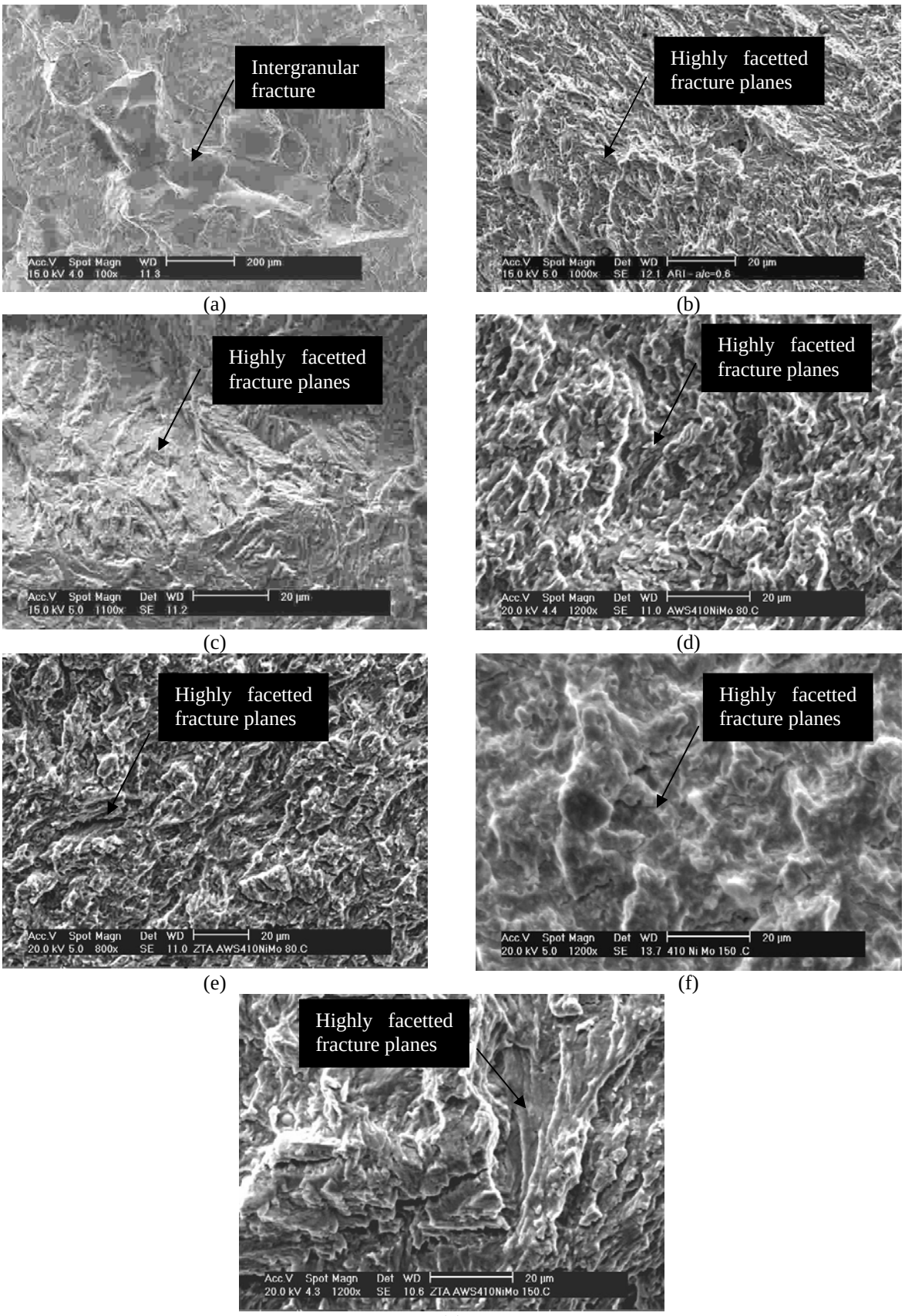

Figure 8. Fractography of low Δ*K* area of CA6NM (a), FCAW WM (b), FCAW HAZ (c), GTAW 80ºC WM and HAZ (d, e), GTAW 150ºC WM and HAZ (f, g).

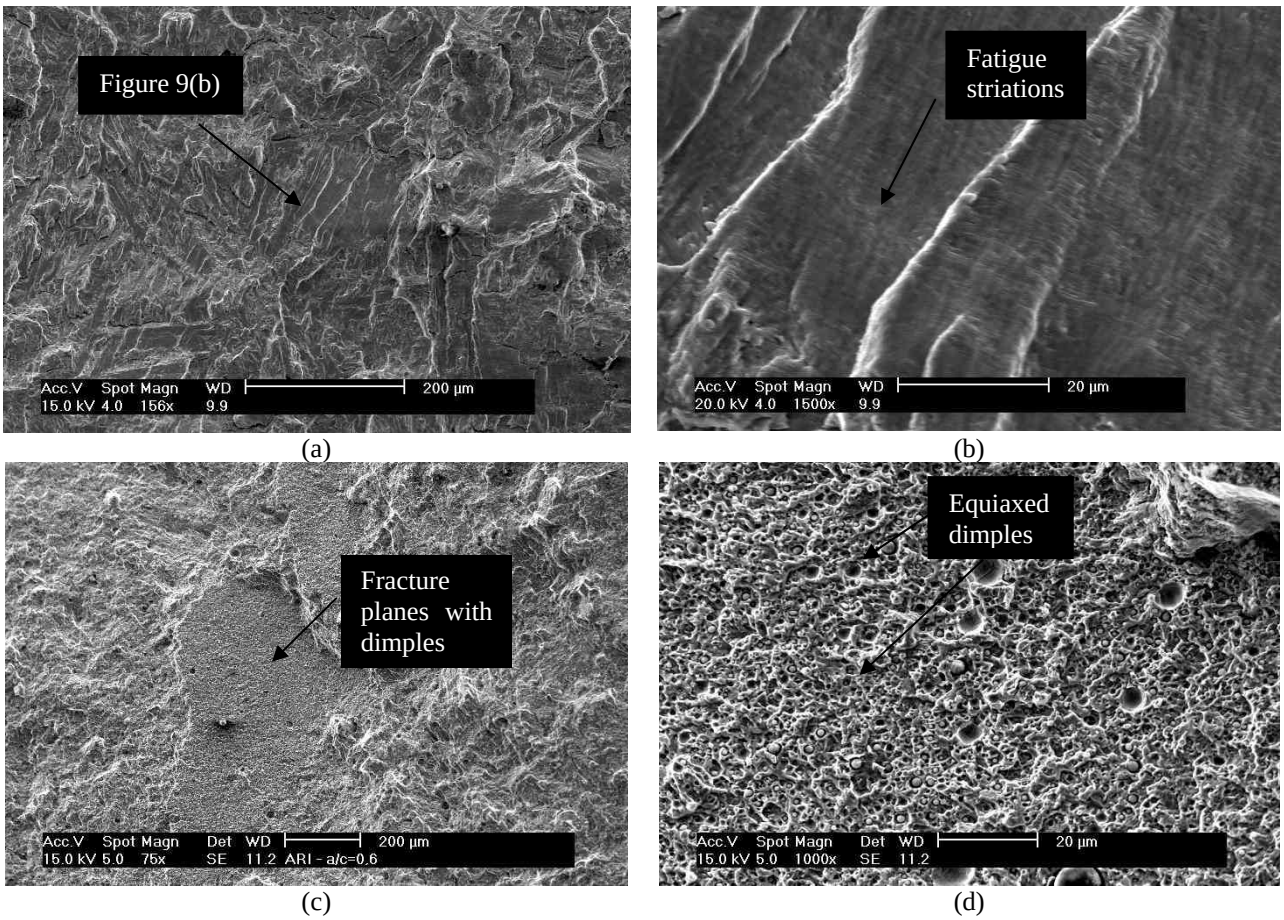

Figure 9. Intermediate Δ*K* fractography area of CA6NM (a) and (b), FCAW WM (c) and (d).

For high Δ*K* values, above of 50 MPa√m, fatigue striations and secondary cracks were observed in all samples with exception to FCAW WM, where it is verified only dimpled fracture. Higher exponent *"m"* of the FCAW WM can be associated with this fracture mechanism, Figure 10. Fatigue striations and secondary cracking are present in CA6NM BM, FCAW and GTAW HAZ fracture surface. In higher Δ*K* values some equiaxied dimples can be observed in GTAW WM welded with 80ºC and 150ºC of interpass temperature .

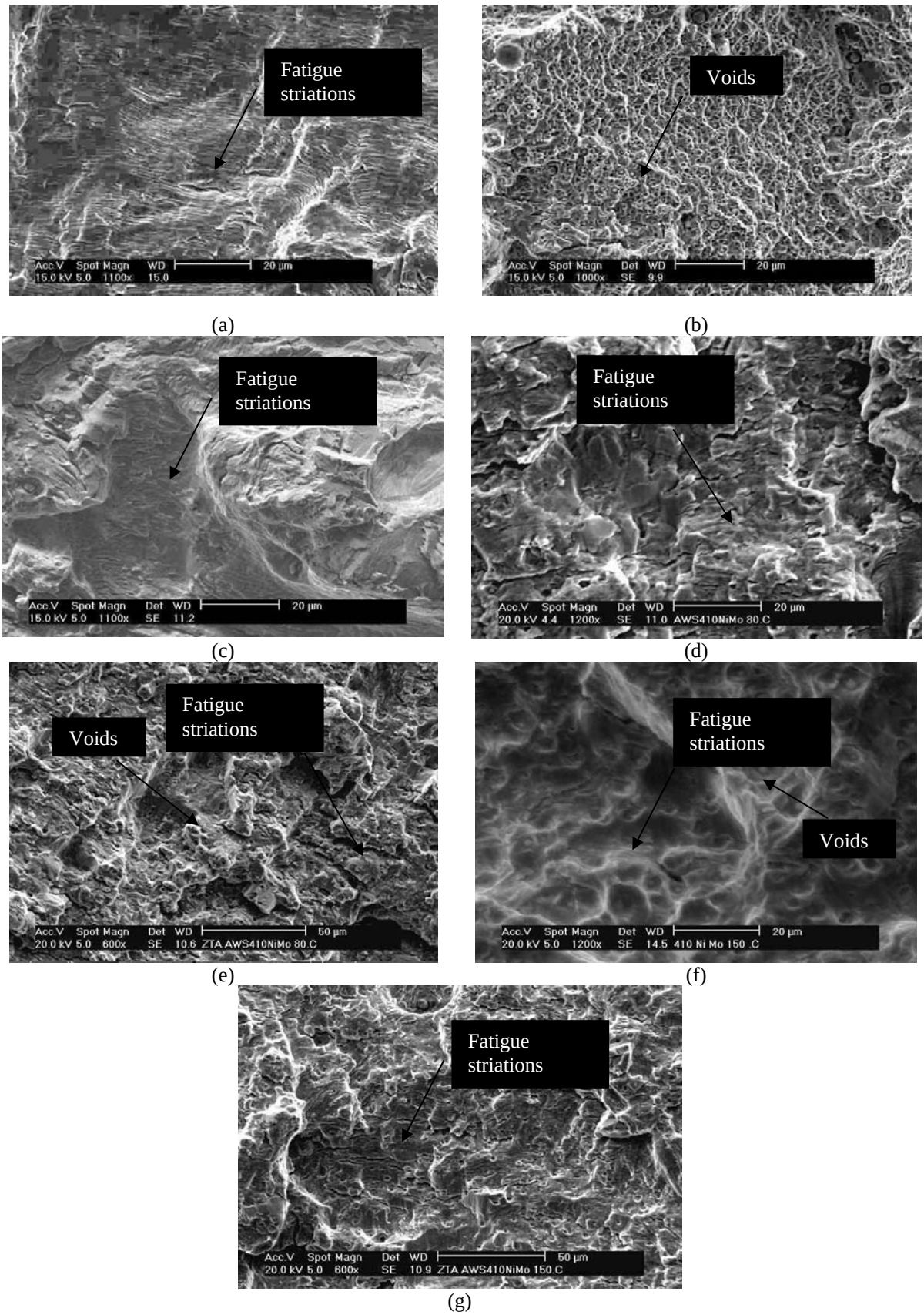

Figure 10. High ΔK fractography area of CA6NM (a), FCAW WM (b), FCAW HAZ (c), GTAW 80ºC WM and HAZ (d, e), GTAW 150ºC WM and ZTA (f, g).

4. Conclusions.

Different fatigue crack propagation behavior was observed in GTAW and FCAW WM, with less fatigue resistance in FCAW WM. Slag inclusions present in the FCAW WM influences the fracture mechanisms and the fatigue crack growth, and promote an increase in the fatigue crack growth rate as well as the *m* exponent of the Paris law.

GTAW welded joints shows similar behavior with CA6NM base material. Better fatigue resistance, was obtained in sample welded with 80ºC interpass temperature. However GTAW HAZ 80ºC shows a little reduction in fatigue crack resistance compared with 150ºC interpass temperature sample.

Fracture mechanisms observed in CA6NM fractured samples were intergranular and highly facetted crack planes, for low ΔK, fatigue striations were observed in intermediate and high ΔK values. Highly facetted crack planes and fatigue striations were observed in FCAW HAZ and GTAW WM and HAZ, with equiaxied dimples in FCAW WM from low ΔK until the final rupture.

5. Acknowledgements

The authors thank the financial support of the Institute of Technology for Development, LACTEC and Companhia Paranaense de Energia Elétrica, COPEL, and the use of laboratory support of the Federal University of Paraná, UFPR and LACTEC.

6. Referências Bibliográficas.

Akhtar, A., Brodie, N. W., Field welding large turbine runners, Water Power & Dam Construction, September, p. 40-46, 1979

American Standard for Testing and Materials, ASTM, ASTM E647–95a: Standard test method for measurement of fatigue crack growth rates.

Bilmes, P.D., Llorente, C.L., Pérez I. J., Toughness and microstructure of 13Cr4NiMo high strength steel welds, Journal of Materials Engineering and Performance, 09, p. 609-615, 2000.

Folkhard, E., Welding Metallurgy of Stainless Steels, Springer-Verlag Wien New York, 1988.

Huth, Hans-Jörg, Fatigue Design of HydraulicTurbine runners, 2005, 178p., Engineering doctor thesis, Norwegian University of Science and Technology, Department of Engineering Design and Materials, Trodheim, Norway.

Kang, K.J., Song, J.H., Earmme, Y.Y., Fatigue crack growth and closure behavior through a compressive residual stress field, Fatigue Fract. Engng. Mater. Struct., 13, 1, 1-13, 1990.

Lee, H. K., Kim, K. S., Kim, C. M., Fracture resistance of a steel weld joint under fatigue loading, Engineering Fracture Mechanics, 66, 403-419, 2000.

Moltubakk T., Strength mismatch effects on the clivage fracture of the heat affected zone of steel welds, 1999, 112p., Norwegian University of Science and Technology, Department of Machine Design and Materials Technology, Ph.D. Thesis, Trondheim Norway.

Pukasiewicz, A.G.M., Propagação de trincas por fadiga em juntas soldadas do aço inoxidável martensítico tipo CA6NM, 2002, Universidade Federal do Paraná, Dissertação de Mestrado em Engenharia de Materiais, Curitiba-PR, Brasil.

Sánchez-Cabrera, V.M., Rubio-Gonzalez, C., Ruíz-Vela, J.L., Ramírez-Baltazar, C., Effect of preheating temperature and filler metal type on the microstructure, fracture toughness and fatigue crack groth os stainless steel welded joints, Materials Science and Engineering A, 452-453, 235-243, 2007.

Shanmugam, K., Lakshminarayanan, V., Balasubramaniam, V., Effect of weld properties on fatigue crack growth behaviour of gas tungsten arc welded AISI 409M grade ferritic stainless steel joints, International Journal of Pressure Vessels and Piping, 2009, doi:10.1016/j.ijvp.2009.02.002.

Shi, Y.M., Chen, B.Y., Zhang, J.X., Effects of welding residual stresses on fatigue crack growth behavior in butt welds of a pipeline steel, Eng Fract Mech, 36, 6, 893-902, 1990.

Tsay, L. W., Liu, C. C., Chao, Y. H., Shieh, Y. H., Fatigue crack Propagation in 2,25 Cr- 1,0 Mo steel weldments in air and hydrogen, Materials Science and Engineering, A299, p. 16-26, 2001.